2009

# Hyaluronidase Activity of Human Hyal1 Requires Active Site Acidic and Tyrosine Residues

Ling Zhang
*University of Nebraska-Lincoln*

Alamelu G. Bharadwaj
*University of Nebraska-Lincoln*

Andrew Casper
*University of Nebraska - Lincoln*

Joel Barkley
*University of Nebraska-Lincoln*

Joseph J. Barycki
*University of Nebraska-Lincoln*, jbarycki2@unl.edu

***See next page for additional authors***

THE JOURNAL OF BIOLOGICAL CHEMISTRY VOL. 284, NO. 14, pp. 9433–9442, April 3, 2009


# Hyaluronidase Activity of Human Hyal1 Requires Active Site Acidic and Tyrosine Residues*[S]

Received for publication, January 12, 2009, and in revised form, February 5, 2009 Published, JBC Papers in Press, February 6, 2009, DOI 10.1074/jbc.M900210200

**Ling Zhang, Alamelu G. Bharadwaj, Andrew Casper, Joel Barkley, Joseph J. Barycki, and Melanie A. Simpson**[1]

*From the Department of Biochemistry, University of Nebraska, Lincoln, Nebraska 68588-0664*

**Hyaluronidases are a family of endolytic glycoside hydrolases that cleave the β1–4 linkage between *N*-acetylglucosamine and glucuronic acid in hyaluronan polymers via a substrate-assisted mechanism. In humans, turnover of hyaluronan by this enzyme family is critical for normal extracellular matrix remodeling. However, elevated expression of the Hyal1 isozyme accelerates tumor growth and metastatic progression. In this study, we used structural information, site-directed mutagenesis, and steady state enzyme kinetics to probe molecular determinants of human Hyal1 function. Mutagenesis of active site residues Glu$^{131}$ and Tyr$^{247}$ to Gln and Phe, respectively, eliminated activity at all hyaluronan concentrations (to 125 μM or 2.5 mg/ml). Conservative mutagenesis of Asp$^{129}$ and Tyr$^{202}$ significantly impaired catalysis by increases of 5- and 10-fold in apparent $K_m$ and reductions in $V_{max}$ of 95 and 50%, respectively. Tyr$^{247}$ and Asp$^{129}$ are required for stabilization of the catalytic nucleophile, which arises as a resonance intermediate of *N*-acetylglucosamine on the substrate. Glu$^{131}$ is a likely proton donor for the hydroxyl leaving group. Tyr$^{202}$ is a substrate binding determinant. General disulfide reduction had no effect on activity in solution, but enzymatic deglycosylation reduced Hyal1 activity in a time-dependent fashion. Mutagenesis identified Asn$^{350}$ glycosylation as the requisite modification. Deletion of the C-terminal epidermal growth factor-like domain, in which Asn$^{350}$ is located, also eliminated activity, irrespective of glycosylation. Collectively, these studies define key components of Hyal1 active site catalysis, and structural factors critical for stability. Such detailed understanding will allow rational design of enzyme modulators.**

Hyaluronidase family enzymes are broadly expressed across many diverse species from bacteria to mammals (1, 2). Depending on the organism, there may be one or several isozymes (3). In humans, five isozymes have been identified and characterized to varying extents for tissue and cellular distribution, activity profile, substrate specificity and function. Hyaluronidases have been termed spreading factors because of their potential to accelerate the spread of toxic venom effects from bees and snakes (4). Loss of hyaluronidase expression in humans is implicated in dysregulated extracellular matrix turnover and correlates with a type of lysosomal storage disorder called mucopolysaccharidosis IX (5). Increased hyaluronidase activity may be important for promotion of vascular development during embryogenesis and wound healing, as well as tumor growth and metastasis (6–13). Because the hyaluronidase expression level and/or activation state is thought to determine whether its effect is to promote or suppress these processes (14), it is critical to gain a thorough understanding of the molecular determinants of its enzymatic activity.

Human hyaluronidases are glycoside hydrolase enzymes (Family 56 as described by the carbohydrate-active enzymes data base at www.cazy.org (15)) characterized by substrate-assisted catalytic mechanism and retention of configuration at the anomeric carbon subsequent to cleavage of the β1–4 linkage between the *N*-acetylglucosamine and glucuronic acid components of the hyaluronan (HA)[2] polymer (1, 16, 17). Members of this family are endoglycosidases, with homology to chitinases and lysozyme (18–21). Several of them, including Hyal1 (22–24), exhibit an acidic activity profile, consistent with their lysosomal function. Scheme 1 illustrates the proposed reaction mechanism, indicating specific acidic amino acid residues directly implicated in catalysis by sequence conservation and homology to the experimentally characterized sperm acrosomal hyaluronidase, PH-20 (25). Much of the proposed scheme has been tested in related enzymes, the chitinases (17–21), because no molecular characterizations of Hyal1 have been performed. Briefly, in the resting state at its optimal pH of 4.0, aspartate 129 and glutamate 131 essentially share a proton. Catalysis is thought to require initiation by intramolecular resonance of the amide bond of *N*-acetylglucosamine in the bound HA polymer. The transition state briefly acquires a positive charge on the nitrogen, whereas the carbonyl becomes an oxyanion nucleophile positioned to attack the electrophilic anomeric carbon of the same *N*-acetylglucosamine unit. As this intramolecular attack occurs, a five-membered ring forms, driving out the C4 hydroxyl of the departing, newly cleaved portion of the chain, which is protonated by Glu$^{131}$. Transition state formation is stabilized by the negative charge on Asp$^{129}$ that is positioned in hydrogen bond distance to the positively charged substrate nitrogen as Glu$^{131}$ transfers its proton to the leaving group. Glu$^{131}$, thus deprotonated, serves to activate an incoming water molecule for hydrolysis of the intramolecular intermediate to restore *N*-acetylglucosamine. Support for this mechanism derives from the observation that allosamidin, an

* This work was supported, in whole or in part, by National Institutes of Health Grants R01 CA106584 and NCRR P20 RR018759 (to M. A. S.).

[S] The on-line version of this article (available at http://www.jbc.org) contains supplemental Fig. S1 and Table S1.

[1] To whom correspondence should be addressed: N246 Beadle Center, Lincoln, NE 68588-0664. Tel.: 402-472-9309; Fax: 402-472-7842; E-mail: msimpson2@unl.edu.

[2] The abbreviations used are: HA, hyaluronan; Hyal, hyaluronidase; DTT, dithiothreitol; PDB, protein data base; EGF, epidermal growth factor; PNGase F, protein *N*-glycosidase F.

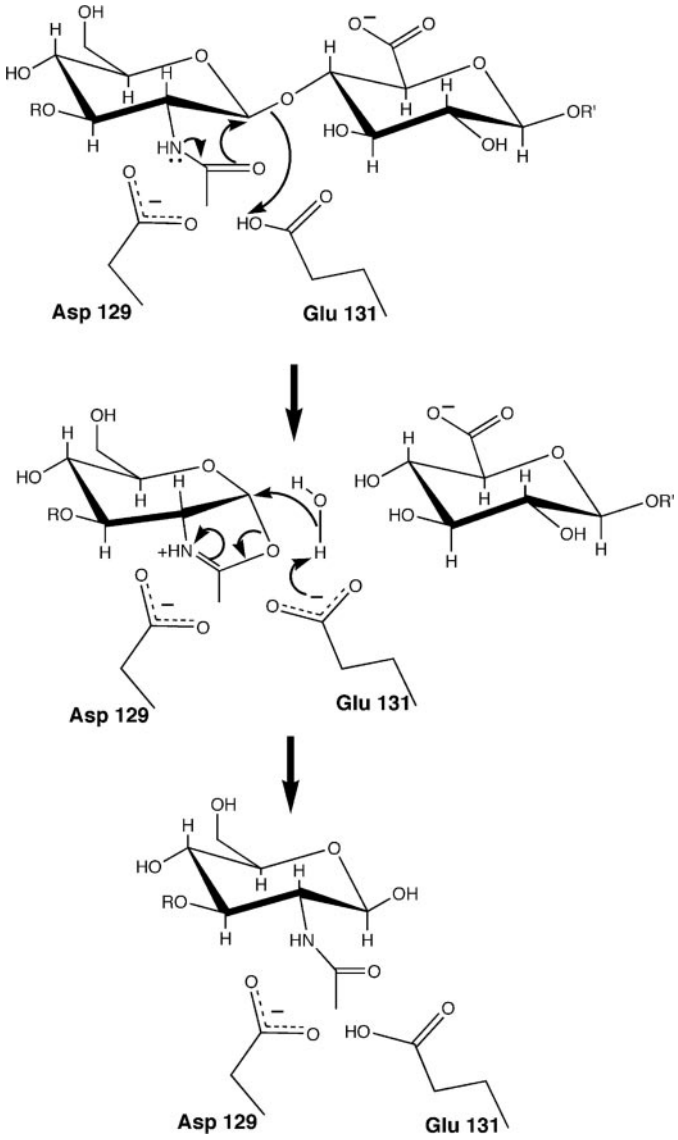


SCHEME 1

oligosaccharide that terminates in a five-membered ring structure, is an effective competitive inhibitor of the closely related chitinase family (21), which cleaves poly-*N*-acetylglucosamine and shows conservation of several key active site residues, including the aspartate and glutamate. Retention of configuration at the anomeric carbon has been shown for a related bacterial *N*-acetylglucosaminidase enzyme (18), and serves to support existence of an intramolecular transition state. Also available is a crystal structure of a distantly homologous bacterial hyaluronan lyase with bound ascorbate, a potent five-membered ring-containing inhibitor of both bacterial lyases and human hyaluronidases (24, 26).

Recently, the crystal structure for human Hyal1 was determined (27). Superposition of available crystal coordinates for a HA tetrameric substrate bound to the bee venom hyaluronidase (4) allowed us to visualize the positions of aspartate and glutamate in hydrogen bond distance of each other and to predict their proximity to the HA tetrasaccharide substrate. We used this structural information, in conjunction with sequence alignments and comparisons to the bee venom hyaluronidase structure, to identify putative active site residues and other structural contributors. A steady state kinetic assay allowed us to quantitatively assess the effects of site-directed mutagenesis, disulfide reduction, and *N*-glycoside removal. These studies collectively provide insights into the respective roles of these features in Hyal1 catalysis.

## EXPERIMENTAL PROCEDURES

*Cell Culture, Materials, and Reagents*—22Rv1 human prostate adenocarcinoma cells (28) and HEK293 human embryonic kidney cells were purchased from ATCC and cultured as directed by the vendor. The pFlag-CMV-3 vector, anti-FLAG M2 antibody-conjugated resin, human umbilical cord HA, Alcian blue, protease inhibitor mixture, bovine serum albumin, tetramethylbenzidine, *N*-acetyl-D-glucosamine, and 4-(dimethylamino)benzaldehyde were purchased from Sigma. Sodium hyaluronate (20 kDa) was from Lifecore Biomedical Inc. (Chaska, MN). Anti-FLAG M2 antibody was purchased from Stratagene (La Jolla, CA). Transient transfection of 22Rv1 and HEK293 cells used the FuGENE 6 transfection reagent (Roche Diagnostics) and calcium phosphate precipitation methods, respectively. Biotinylated HA-binding protein was from Seikagaku (Associates of Cape Cod, East Falmouth, MA), *Streptomyces* hyaluronidase was from EMD Biosciences (San Diego, CA), protein *N*-glycosidase (PNGase F) was from New England Biolabs (Ipswich, MA).

*Substrate Modeling and Structure Representation*—We modeled human Hyal1 in complex with bound HA tetrasaccharide substrate by superimposing coordinates for the published *Apis melliflora* hyaluronidase-HA complex (PDB accession 1FCV (4)) onto the coordinates for human apo-Hyal1 (PDB accession 2PE4 (27)). A ribbon rendering of the model was made with Chimera (29). To facilitate selection of residues specifically involved in catalysis, the active site of a modeled complex with a HA tetrasaccharide was centered upon as depicted in Fig. 1. Side chains with potential for chemical reactivity within 5 Å of the cleaved HA glycoside were identified, as well as several additional residues that lined the groove possibly accommodating the full substrate. Conservation across human, bovine, murine, and bee species in sequence alignments of all hyaluronidase isozymes was used as an additional criterion to refine our choice of putative catalytic, substrate binding and structural residues. Upon determining that removal of *N*-glycosides negatively impacted activity, we additionally identified three putative *N*-glycosylation sites by primary sequence analysis using NetNGlyc (30), which are largely conserved among human hyaluronidases but not broadly across species. The side chains for residues examined in the study were colored by atom.

*Generation and Purification of Hyal1 Point Mutants*—For Hyal1 overexpression, we utilized the pFlag-CMV-3 eukaryotic vector encoding the preprotrypsin extracellular secretion signal followed by a FLAG epitope tag fused to the coding sequence for Hyal1 with the 21-amino acid signal peptide removed. The preprotrypsin signal peptide ensured abundant soluble FLAG-tagged Hyal1 secretion to the conditioned cell culture media of transfectants. Point mutants of Hyal1 were generated from the wild-type pFlag-Hyal1 construct using the

QuikChange site-directed mutagenesis kit (Stratagene) according to the manufacturer's protocol. Primer sequences used to create the wild-type construct and specific point mutations are given in supplemental Table S1 (affected codons are highlighted). Coding sequences for D129N, E131Q, Y202F, N216A, S245A, Y247F, and R265L, N350A, N350tr, and L356tr were verified by the Genomics Core at the University of Nebraska-Lincoln.

For initial activity measurements, recombinant plasmids encoding N-terminal FLAG epitope fusions to Hyal1 and the point mutants were used to transfect human 22Rv1 prostate carcinoma cells with FuGENE 6. After 48 h in RPMI containing 1% serum, conditioned media were collected and concentrated 10-fold using Centriplus YM-10 microconcentrators. Protease inhibitor mixture was added to the final concentrated supernatant. Soluble expression of wild-type and mutant Hyal1 was verified by Western analysis with anti-FLAG M2 antibody.

Wild-type and mutant protein used for measurement of kinetic constants and evaluation of post-translational modifications was purified from conditioned media of HEK293 transfectants, with the exception of the N350A, N350tr, and L356tr mutants, which were purified from the soluble fraction of HEK293 cell lysates. Media were harvested 48 h after calcium phosphate transfection, concentrated at least 10-fold, and dialyzed exhaustively against 1× Tris-buffered saline before applying to anti-FLAG affinity resin. After washing with 10 column volumes of Tris-buffered saline, Hyal1-FLAG was eluted from the column with FLAG peptide and dialyzed against hyaluronidase assay buffer (50 mM sodium formate, pH 4.0, 150 mM NaCl). Folded structure of mutants that lacked activity was implied by soluble secretion, but also by their intrinsic tryptophan fluorescence profiles (31), which were identical to those of wild-type Hyal1, and red-shifted comparably upon denaturation with 3 M guanidine-HCl (supplemental Fig. S1).

*Evaluation of Post-translational Modifications*—To evaluate the importance of disulfides, purified Hyal1 was incubated in the absence or presence of 1, 10, or 50 mM DTT, or 5 mM β-mercaptoethanol, for 1 h at 37 °C prior to activity analysis. The importance of *N*-glycosides to Hyal1 activity was examined by enzymatic removal. Purified Hyal1 (16 μg) was incubated with 10 units of PNGase F, which is specific for protein *N*-glycoside digestion, in the vendor's recommended buffer (50 mM sodium phosphate, pH 7.5, 1% Nonidet P-40) for the indicated times prior to Western blot and kinetic assay.

*Hyaluronidase Activity Assays*—Hyal1 activity was measured by one of three methods. Substrate gel electrophoresis was performed essentially as previously described (32). Concentrated conditioned media were electrophoresed by SDS-PAGE on a 10% polyacrylamide gel containing 0.2 mg/ml HA. After a 1-h renaturation in 3% Triton X-100, gels were incubated in hyaluronidase assay buffer at 37 °C overnight, stained with 0.5% Alcian blue for at least 2 h, and destained with 7% acetic acid.

Initial quantitative comparisons of wild-type and mutant Hyal1 activity were done in an HA-coated microplate assay (13, 32–34). Briefly, serial dilutions of concentrated conditioned media adjusted for equal Hyal1 content were applied in triplicate to 96-well plates that had been precoated overnight at 4 °C in a solution of 50 μg/ml human umbilical cord HA (200 mM carbonate buffer, pH 9.6), and blocked with Pierce Superblock reagent. After a 1-h incubation in hyaluronidase assay buffer, wells were washed and residual HA was detected by biotinylated HABP, detected with avidin-biotin horseradish peroxidase and tetramethylbenzidine substrate. Absorbance at 650 nm was used to interpolate specific activity from a concurrent *Streptomyces* hyaluronidase standard curve.

Activity of wild-type and all mutant Hyal1 species was assayed as previously described by Reissig *et al.* (36). Purified enzyme (0.5 μg) was incubated with increasing concentrations of HA (20 kDa) in hyaluronidase assay buffer containing 0.1% bovine serum albumin. The reaction was heat inactivated (100 °C for 5 min). Cleaved ends were quantified by the Morgan-Elson color reaction (potassium tetrahydroborate and acidified dimethylamino benzaldehyde) and absorbance at 585 nm. Molar quantity of *N*-acetylglucosamine reducing ends in each sample was interpolated from a concurrently developed standard of *N*-acetyl-D-glucosamine. An initial time course revealed linear kinetics for wild-type Hyal1 from 10 to 90 min, so a time point of 60 min was chosen for all subsequent assays. Michaelis constants ($K_m$ and $V_{max}$) were determined for Hyal1 species that exhibited saturable kinetics by fitting data to a model of single site association using Prism (GraphPad Software Inc., La Jolla, CA). Heterogeneous viscosity of the HA solutions increased above 125 μM (2.5 mg/ml), so this was the maximum concentration assayed. Thus, $K_m$ and $V_{max}$ values were extrapolated from the curve fit where indicated.

## RESULTS

*Examination of the Hyal1 Active Site*—Our goal in this study was to probe the molecular interactions that specify hyaluronidase activity of human Hyal1. To obtain sufficient protein quantities, we overexpressed the enzyme as a secreted N-terminal FLAG epitope fusion. Because a significant aspect of research on Hyal1 is focused in the context of human cancer, we initially used 22Rv1, a human prostate adenocarcinoma cell line model for prostate cancer progression, as the host line for protein production. These cells normally produce little active hyaluronidase (13), and overexpression of Hyal1 was found to accelerate their growth in culture as well as their metastatic dissemination to lymph nodes in mouse orthotopic tumor models (6, 37). Abundant soluble FLAG-tagged Hyal1 was secreted to the conditioned cell culture media of transfectants.

The first round of mutagenesis was directed at characterization of the putative enzyme active site. Using crystal coordinates for the bee venom hyaluronidase complexed with HA (4), in conjunction with human apo-Hyal1 coordinates (27), we depicted the human enzyme bound to a tetrasaccharide substrate, and inspected the architecture of the active site (Fig. 1). Based on this model, we identified specific residues within 5 Å of the cleaved HA product in the active site, as likely to be important for catalytic activity. We further selected several amino acids that lined a groove capable of accommodating a full-length HA polymer prior to cleavage. Accordingly, point mutations were generated at residues $Asp^{129}$, $Glu^{131}$, $Tyr^{202}$, $Asn^{216}$, $Tyr^{247}$, $Ser^{245}$, and $Arg^{265}$ to investigate their individual contributions to the enzyme mechanism. Fig. 1 illustrates the positions of these residues in the active site of human Hyal1

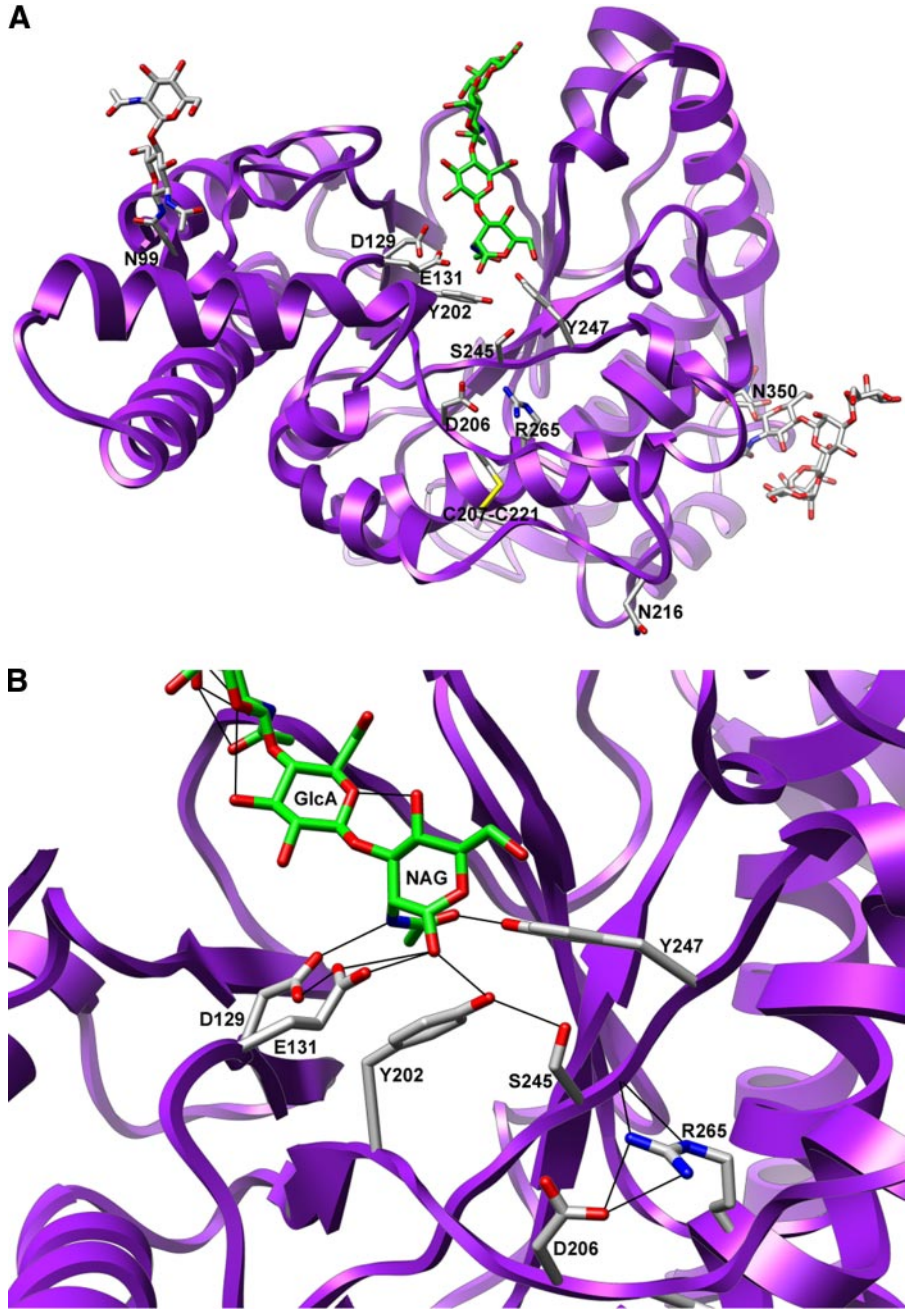


FIGURE 1. **Ribbon representation of the human Hyal1 crystal structure with bound HA tetrasaccharide.** Crystal coordinates from the HA substrate crystallized in the bee venom hyaluronidase structure (PDB code 1FCV) were used to place an HA tetrasaccharide in stick representation at the active site groove of human Hyal1 (PDB code 2PE4). *A*, side chains of residues examined in this study for potential catalytic importance are labeled and shown in stick representations. One active site proximal disulfide is indicated ($Cys^{207}$–$Cys^{221}$), as well as the three asparagines that are sites for *N*-glycosylation ($Asn^{99}$, $Asn^{216}$, and $Asn^{350}$), shown modified with short carbohydrate chains as determined in the crystal structure. The molecular interactions occurring between bound HA and putative catalytic residues at the active site are depicted in an active site magnification (*B*), with hydrogen bonds indicated by *thin black lines*. Carbon atoms of the protein residues and modifications are represented in *gray*, whereas those of the substrate are in *green*. In both cases, nitrogen atoms are *blue*, oxygen are *red*, and sulfurs are *yellow*. *GlcA*, glucuronic acid; *NAG*, *N*-acetylglucosamine.

relative to HA. Substrate-proximal residues fell into three regions: residues still in contact with the residual tetrasaccharide that can be presumed involved in binding and substrate recognition; residues in non-covalent bond distance from the newly cleaved end of the substrate, including $Asp^{129}$ and $Glu^{131}$, that are obvious candidates for direct catalytic roles; and residues proximal to the cleavage point of the substrate that were likely to have been in contact with a transition state and/or the released portion of the cleaved HA chain, such as $Tyr^{202}$ and $Tyr^{247}$. Analogy to point mutations in both sperm hyaluronidase, PH-20 (25), and bacterial *N*-acetylglucosaminidase H (20), further suggested $Asp^{129}$ and $Glu^{131}$ would be critical for catalytic activity of the enzyme. $Arg^{265}$ has previously been predicted to be important for substrate binding. $Asn^{216}$ is a putative *N*-glycosylation site and its placement within the substrate groove led us to test its importance for enzyme activity and/or substrate binding. The roles of the serine and tyrosine residues have not been examined in any hyaluronidases.

Wild-type and all Hyal1 point mutants were expressed and secreted to conditioned media (Fig. 2*A*). Initial characterization of enzyme activities was performed at a single HA concentration in HA-coated microwell plates, using concentrated culture media from transfected tumor cells (Fig. 2*B*). Results of these assays demonstrated negligible activity for the E131Q mutant (0.11 ± 0.01 units/ml of culture media per mg of Hyal1), similar to the vector-transfected control media (NC, 0.07 ± 0.01 units/ml/mg). This value is 0.26 ± 0.03% of wild-type Hyal1 activity. Catalytic function was also significantly diminished by D129N mutagenesis (1.4 ± 0.3% of wild-type activity), as well as Y202F (5.6 ± 1.4%), Y247F (4.8 ± 0.7%), and R265L (1.4 ± 0.6%). S245A retained 36 ± 6% of normal activity, whereas N216A had no effect. The relative effects on activity were also observed when soluble lysates from the respective transfectants were assayed in the microplate format (data not shown). Thus, the acidic and tyrosine residues, as well as serine 245 and arginine 265, appeared to have prominent roles in the hyaluronidase activity of Hyal1. To address the specific functions of individual residues more rigorously, we subsequently purified each Hyal1 species from HEK293 transfectant media, because these cells were more easily transfected and yielded greater protein quantities.

*Glutamate 131 and Tyrosine 247 Are Essential Catalytic Residues*—For kinetic analyses, we measured Hyal1 activity by the method of Reissig *et al.* (36), in which cleavage events are quantified by the reaction of liberated *N*-acetylglucosamine ends with a colorimetric substrate. Activity of the wild-type enzyme was saturable with increasing substrate concentration (Fig. 3*A*). Apparent kinetic constants $K_m$ and $V_{max}$ were calculated by non-linear curve fitting of the data to an equation for single site association, considering all HA substrate and product sizes equally (Table 1). Activity values for each mutant at the 50 $\mu$M coating concentration used in the microplate assay were also compared with those of the wild-type enzyme. Analysis of E131Q kinetics revealed no significant activity at any HA concentration tested, even with 5-fold more enzyme added (Fig. 3*B*). This is consistent with results from the analogous PH-20 hyaluronidase mutant assayed by agarose gel electrophoresis (25) and with the above microplate assay. Although several of the mutants (*i.e.* D129N and Y202F, Fig. 3*C*, discussed below) showed clear dependence of activity on substrate concentration, E131Q did not. Identical results were observed with the Y247F mutant (Fig. 3*D*). Absence of activity at all substrate concentrations indicates $Glu^{131}$ and $Tyr^{247}$ have critical roles in the catalytic mechanism.

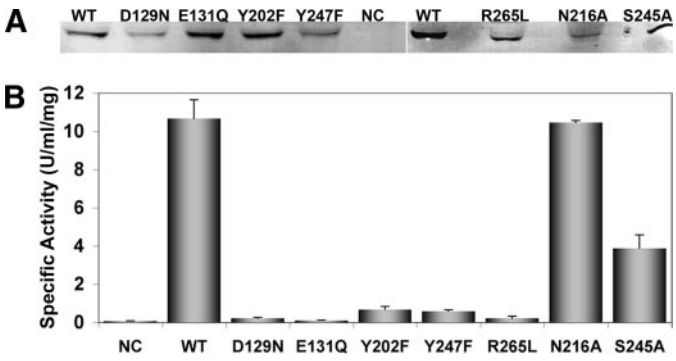


FIGURE 2. **Conservative mutagenesis of specific acidic and tyrosine residues significantly reduces Hyal1 activity.** The indicated mutations were introduced to the wild-type pFlag-Hyal1 construct as described under "Experimental Procedures." Conditioned media were prepared from 22Rv1 human prostate tumor cells transfected with the respective constructs. *A*, equivalent protein amounts, as determined by Bio-Rad assay, were analyzed by Western blot probed with anti-FLAG antibody to compare wild-type and mutant Hyal1 expression. *B*, hyaluronidase activity of the conditioned media was assayed in a quantitative microplate assay. Densitometric measurements from the Western blot in *A* were used to normalize wild-type and mutant Hyal1 content. Equal amounts of the indicated Hyal1 species were serially diluted and applied in triplicate to HA precoated microwell plates. Residual HA was quantified to obtain specific activities. Values represent the mean ± S.E.

*Aspartate 129 Directly Supports Catalysis, Whereas Tyrosine 202 and Serine 245 Are Substrate Binding Determinants*—In addition to $Glu^{131}$, $Asp^{129}$ was also predicted to be an essential catalytic residue. Mutagenesis of this residue to the isosteric asparagine significantly reduced $V_{max}$ and increased $K_m$ nearly 5-fold (Fig. 3*C* and Table 1). Interestingly, $Asp^{129}$ was not essential, because significant activity was retained. Detrimental effects specifically resulting from loss of its acidic character suggest a direct catalytic function, whereas change in $K_m$ implicates $Asp^{129}$ additionally in HA binding. Based on their respective positions, $Tyr^{202}$ and $Ser^{245}$ were predicted to position the substrate acetamido group for attack on the anomeric carbon. Kinetic analysis showed that Y202F reduced but did not eliminate enzyme activity (Fig. 3*C*). However, its clear role in hydrogen bond coordination of the substrate and placement of other residues at the active site is reflected in the $K_m$ for substrate that is increased ≈10-fold relative to that of the wild-type enzyme. Catalysis by S245A is unaltered with respect to $V_{max}$, but this mutant has lower affinity for HA as indicated by the ≈3-fold higher $K_m$ (Fig. 3*A* and Table 1). Thus, the importance of $Ser^{245}$ at the enzyme active site is to ensure substrate binding. Collectively, these conserved residues are important for maximal catalytic efficiency, although they are not essential for function.

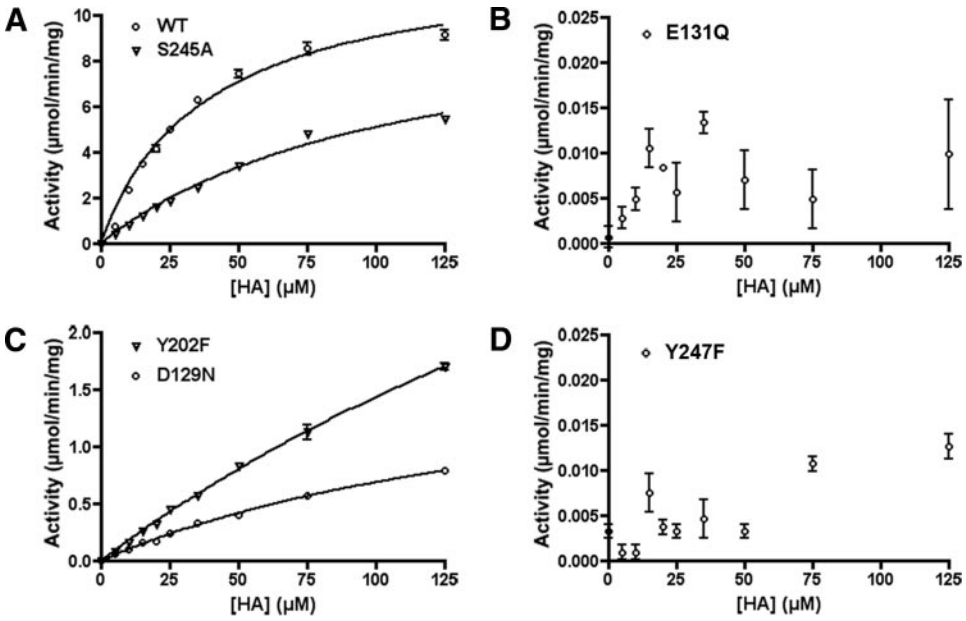


FIGURE 3. **Kinetic analysis of wild-type and mutant Hyal1 reveals the importance of active site residues in substrate affinity as well as catalysis.** Purified protein was incubated for 60 min with the indicated concentrations of sodium hyaluronate (*HA*, 20 kDa) before quantification of cleavage events by Morgan-Elson color reaction as described under "Experimental Procedures." Data were fitted to an equation for single site association and used to calculate specific activities, $V_{max}$ and Michaelis constants as presented in Table 1. Mean ± S.D. of triplicate determinations for each HA concentration were plotted with the curve fit. Results for Hyal1 species that exhibited saturable kinetics in the conditions evaluated are shown: *A*, Hyal1 wild-type (*WT*) and S245A point mutant (0.5 $\mu$g of enzyme assayed); *C*, Y202F and D129N (2.5 $\mu$g of enzyme), plotted on a different scale to illustrate saturability; *B*, E131Q, and *D*, Y247F had negligible activity at all HA concentrations (2.5 $\mu$g of enzyme).

*Alteration of Arginine 265 Perturbs Active Site Architecture*—Kinetic analysis of the R265L mutant confirmed a significant reduction in enzyme activity, as observed in the microplate assay (Table 1). In fact, this mutation was as disruptive as D129N, retaining only ≈4% of wild-type activity at 50 $\mu$M HA (Table 1). However, dependence of activity on HA concentration was approximately linear over the range tested and did not approach saturation, so

we were unable to determine kinetic constants for this mutant. At the maximum HA concentration of 125 $\mu$M (2.5 mg/ml), activity was 0.67 ± 0.02 $\mu$mol/min/mg, which was 7.3% of the wild-type enzyme activity at this amount. Thus, catalytic function was impaired within this range of HA concentrations, but it was not possible to predict whether $V_{max}$ was altered.

**TABLE 1**
**Summary of Hyal1 wild-type (WT) and mutant kinetic constants**

| Enzyme | $K_m$ | $V_{max}$ | % WT activity at 50 $\mu$M HA |
|---|---|---|---|
| | $\mu$M | $\mu$mol/min/mg | |
| Hyal1 wild-type | 38.1 ± 4.8 | 12.5 ± 0.7 | 100.0 ± 1.8 |
| **Catalytic mutants** | | | |
| E131Q | NA[a] | NA | 0.08 ± 0.01 |
| Y247F | NA | NA | 0.04 ± 0.01 |
| D129N | 181 ± 19[b] | 1.9 ± 0.1[b] | 5.10 ± 0.09 |
| **Substrate binding mutants** | | | |
| Y202F | 367 ± 37[b] | 6.7 ± 0.5[b] | 11.1 ± 0.0 |
| S245A | 110 ± 19 | 10.7 ± 1.1 | 41.1 ± 0.4 |
| **Putative structural mutants** | | | |
| R265L | NS[c] | NS | 4.18 ± 0.09 |
| N216A | 103 ± 14 | 10.0 ± 0.8 | 44.6 ± 1.3 |
| N350A | NS | NS | 0.12 ± 0.01 |
| N350tr | NS | NS | 2.49 ± 0.17[d] |
| L356tr | NS | NS | 6.29 ± 1.50[d] |

[a] NA indicates no measurable activity at any HA concentration.
[b] Indicates extrapolated value from saturable curve fit.
[c] NS, not saturable, indicates data do not fit a saturation curve.
[d] Values measured at 125 $\mu$M HA.

*Disulfide Stabilization Is Not Critical for Activity*—The Hyal1 enzyme contains five disulfide bonds, three of which are located in a C-terminal EGF-like domain remote from the enzyme active site. However, one disulfide bond occurs between $Cys^{207}$ and $Cys^{221}$, both adjacent to the putative substrate binding groove. This disulfide appears to be required for stabilization of a loop containing the $Asn^{216}$ glycosylation site (Fig. 1*A*). Disulfides have been suggested to have importance in the function of PH-20 (38), but their role has not been tested extensively. To test the significance of disulfides for activity of Hyal1, we treated affinity purified protein with the disulfide reducing agent DTT, and evaluated its resulting activity (Fig. 4). Both conditioned media and FLAG-affinity purified Hyal1 contained abundant protein activity. Interestingly, this activity was completely eliminated in a HA substrate gel assay (Fig. 4*B*), whereas no effects were observed in the microplate format (Fig. 4*C*), unless the enzyme was first heat-inactivated. Kinetic analysis revealed identical saturation and Michaelis constants for concentration dependence of specific activity (Fig. 4*D*), consistent with results of the microplate assay. Furthermore, saturation curves and kinetic constants were not affected at any concentration of DTT (1, 10, or 100 mM), nor by preincubation with 5 mM $\beta$-mercaptoethanol (data not shown). Thus, disulfides probably affect folding of the enzyme and long term stability in the acidic environment of the lysosome, but the folded Hyal1 active site does not intrinsically appear to require disulfide bonds for its optimal conformation.

*Deglycosylation of Hyal1 or Mutagenesis of Asparagine 350 Eliminates Activity*—In studies of the PH-20 isozyme, deglycosylation was found to reduce hyaluronidase activity in substrate gel assays (38). Three canonical *N*-glycosylation sites are present in Hyal1. To test their importance, *N*-glycosyl moieties

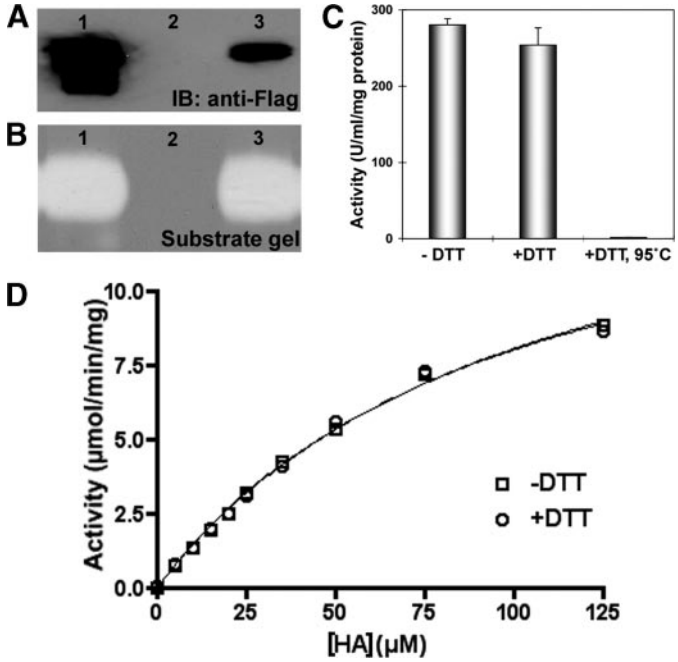


FIGURE 4. **Disulfide bonds are important for the stability but not the activity of intact Hyal1.** FLAG affinity purified Hyal1 (wild-type) was incubated in the absence or presence of 1 mM DTT prior to Western blotting (*A*), HA substrate gel analysis (*B*), or quantification of activity by microplate assay (*C*) and kinetic analysis (*D*), as described under "Experimental Procedures". Lanes in *A* contain: *1*) Hyal1 conditioned media; *2*) anti-FLAG affinity column flow-through; and *3*) eluted Hyal1. In *B*, *lane 1* contains Hyal1 transfectant-conditioned media; *lanes 2* and *3* contain purified Hyal1 with and without 1 mM DTT, respectively. Data plotted are the mean ± S.E. (*C*) and mean ± S.D. (*D*) of triplicate determinations. *D*, the concentration dependence of specific activity was fitted to an equation for single site association. Curve fits are superimposed as indicated for assays in the continuous absence or presence of 1 mM DTT following the initial preincubation period. *IB*, immunoblot.

were digested from purified Hyal1 and activity was assayed relative to extent of glycosylation. Removal of glycosides was monitored concurrently by Western blot (Fig. 5*A*). Significant digestion of glycosides was already evident at 0 h as a shift in molecular masses from a major ≈52-kDa band in the untreated sample, presumably corresponding to the fully glycosylated species, to a series of 4 bands within the first 5 min after PNGase F addition. Despite this apparent shift, the HA dependent activity curve at this time point was superimposable for untreated and treated samples (Fig. 5*A* and data not shown). The 52-kDa band was virtually absent by 2 h and no longer visible at 4 h, replaced by a doublet of ≈42 and ≈45 kDa in the treated samples. Longer digestion times did not alter this pattern. Kinetic analysis showed Hyal1 activity decreased in a time dependent fashion with deglycosylation (Fig. 5*A*), with apparent $V_{max}$ values only 57, 12, and 1.3% of the untreated $V_{max}$ at 1, 2, and 4 h, respectively.

To confirm the importance of the glycosyl moieties in Hyal1 catalytic function, we mutagenized two of the *N*-glycosylation sites. One, $Asn^{216}$, was located in the disulfide-positioned loop that forms part of the extended active site, and the other, $Asn^{350}$, was located in the C-terminal EGF-like domain. Consistent with the non-essential role of disulfide loop positioning in catalysis, the N216A mutant was maximally active in both the microplate assay (Fig. 2*B*) and kinetic analysis (Fig. 5*B*), although its $K_m$ for HA was increased ≈3-fold. *N*-Glycosylation

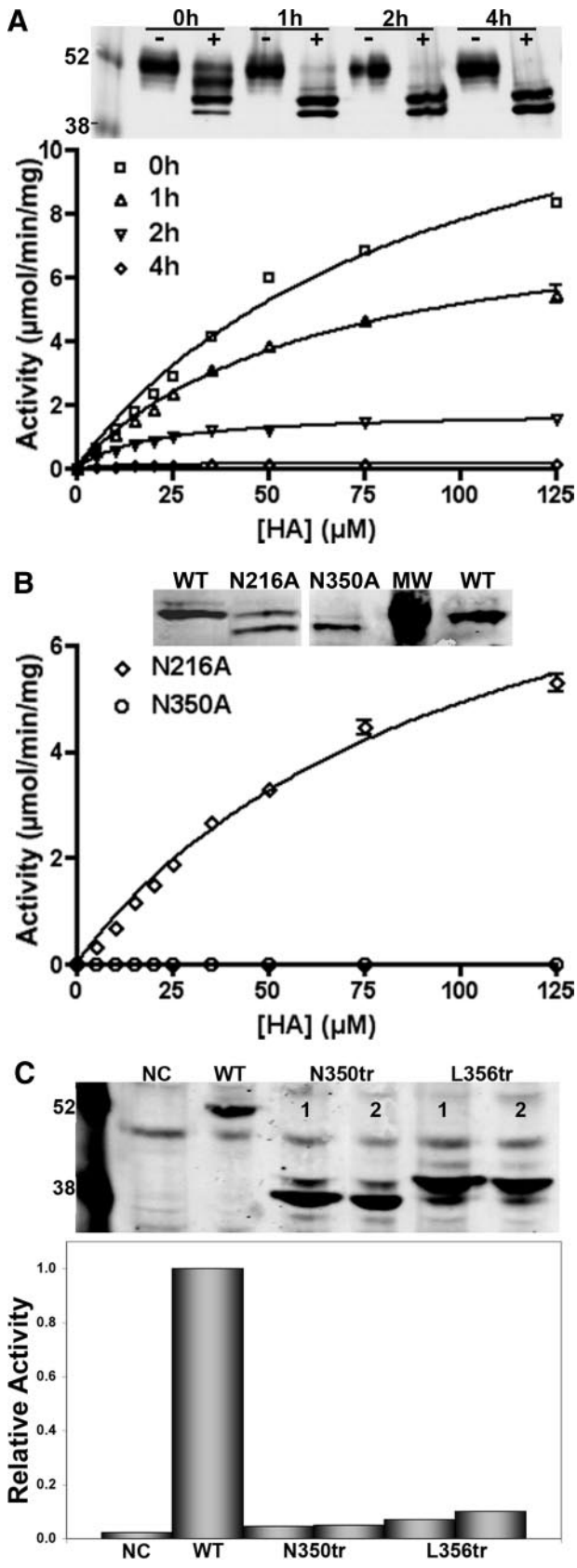


FIGURE 5. **Glycosylation of asparagine 350 is essential for enzyme activity.** *A*, purified Hyal1 (wild-type) was incubated in the absence or presence of PNGase F for 0, 1, 2, or 4 h prior to analysis by Western blot probed with anti-FLAG antibody (*upper panel*) and kinetic assay. Mean ± S.D. and curves fitted to a single site association are shown from triplicate determinations. *B*, site-specific mutations were made to eliminate two of the three *N*-glycosylation sites in Hyal1. Purified protein was compared with wild-type in Western blots probed with anti-FLAG (*upper panel*). *MW* denotes the molecular weight ladder; the band is 52 kDa. The N216A mutant was purified from the conditioned media and kinetic parameters determined exactly as for the wild-type enzyme. The N350A mutant was expressed solubly but was not secreted, so it was purified from the soluble HEK293 cell lysate and used in 5-fold excess for kinetic assay. Mean ± S.D. and curves fitted to a single site association are shown from triplicate determinations. *C*, stop codons were introduced by site-directed mutagenesis of the Hyal1 coding sequence, to generate C-terminal truncations that eliminated the EGF-like domain at (N350tr) or after (L356tr) the $Asn^{350}$ glycosylation site. Western analysis of soluble HEK293 cell lysates from vector (*NC*), Hyal1 wild-type (*WT*), and two separate transfections each of N350tr and L356tr are shown in the *upper panel*. Protein was purified from each lysate and assayed for specific activity at a single HA concentration (125 μM, HA 20 kDa) using the Morgan-Elson color reaction. Activity of each is plotted relative to that of wild-type Hyal1.

at position 216 was not required for expression or extracellular secretion of the enzyme (Fig. 2*A*), but the N216A mutant was observed as a doublet of ≈52 and ≈48 kDa in some preparations (Fig. 5*B*), suggesting variable glycosylation. In contrast, the N350A mutant was expressed only in the soluble cell lysate as a species of ≈48 kDa. The wild-type protein was consistently observed in both media and lysate as a 52-kDa band. Kinetic analysis of the wild-type enzyme affinity purified from the lysate produced activity curves identical to those of Hyal1 from conditioned media (data not shown), but the lysate-purified N350A mutant exhibited negligible activity at any HA concentration tested (≈0.1% of wild-type at 50 μM, Table 1 and Fig. 5*B*).

*Deletion of the EGF-like Domain Abolishes Hyal1 Activity Independently of Asparagine 350*—The C-terminal EGF-like domain is not found in the bacterial or bee venom hyaluronidases, so previous models of Hyal1 using coordinates for the bee venom ortholog depicted this region as an independently folded domain with minimal contacts to the active site containing domain. Inspection of the human Hyal1 model reveals a single overall folded domain, with extensive contacts between the EGF-like region, the sugar moieties of the $Asn^{350}$ glycosyl adduct housed within that region, and the remainder of the protein. We introduced stop codons at position 350 (N350tr), which deleted 86 amino acids, including the $Asn^{350}$ glycosylation site, and at position 356 (L356tr), which deleted the 80-amino acid EGF-like domain but retained $Asn^{350}$. Neither deletion mutant was secreted to the extracellular space but both were expressed well in the soluble lysate (Fig. 5*C*). Western blot showed the N350tr lysates contained a major band of ≈38 kDa, the predicted molecular mass for the polypeptide, whereas the major band in L356tr lysates was ≈42 kDa, consistent with the 4-kDa shift observed for the fully glycosylated wild-type enzyme. The lysates showed ≈2.5 and ≈6.3% of wild-type activity for N350tr and L356tr, respectively, at the 125 μM HA amount. Thus, loss of this domain is deleterious to both secretion and activity of Hyal1, although the residual activity suggests the effect is indirect.

## DISCUSSION

Hyaluronidase enzymes, most extensively Hyal1, have been implicated in normal and pathological extracellular matrix turnover. Crystallographic studies have illuminated the Hyal1 structure (27) and investigation of the wild-type enzyme puri-

fied from insect cells demonstrated its minimum octasaccharide substrate requirement (22). Several naturally occurring inhibitors have been reported, but rational design of high affinity and/or mechanism-based inhibitors to control disease progression requires detailed characterization of Hyal1 chemistry. In particular, specific molecular features conferring enzymatic properties to Hyal1 have not been previously examined. In this report, we confirmed the presumed catalytic roles of two active site residues, identified three additional catalytic components, and characterized several structurally stabilizing features, including the intriguing EGF-like domain.

Typically, hyaluronidase activity has been measured at a single time point and HA concentration. This is useful for detection of small amounts of enzyme in complex mixtures. However, this activity represents a maximum saturation level and cannot be used to compare quantitatively among hyaluronidases. To establish a system for detailed kinetic analysis, it was first necessary to generate large scale expression and purification schemes. Active Hyal1 had been produced previously using insect cell expression systems (22–24), but the sugar content of glycosyl moieties is often not accurately reproduced by insects relative to the human sequences. Because both PH-20 and Hyal1 hyaluronidases have shown sensitivity to glycosylation, the nature of these modifications has the potential to impact enzymatic function. As an alternative, we expressed wild-type and mutant human Hyal1 with a FLAG epitope tag and immunoaffinity purified the resulting protein from the conditioned media of either human prostate carcinoma cells or embryonic kidney cells. Michaelis-Menten kinetic values were not previously determined for Hyal1 but specific activity reported at a given concentration (22, 24) is within an order of magnitude of the values we report here. Using the octasaccharide substrate, saturation was essentially observed within the same range we utilized (22), adjusted for the 10-fold difference in molar mass of the 2-kDa octasaccharide *versus* the 20-kDa polymeric HA substrate. The somewhat lower activity of Hyal1 purified from insect cells relative to the enzyme we have prepared from human cell culture may be due either to differences in utilization of these substrate sizes or in glycosylation.

In studies of PH-20, the residual activity of the analogous mutation to D129N, absent in E131Q, was interpreted in favor of an essential direct role in chemical catalysis for $Glu^{131}$, and a supporting role in transition state stabilization for $Asp^{129}$ (2, 25). It is clear that the acidic character of the residue is critical in both cases. This observation is also consistent with the mechanism illustrated in Scheme 1, in which protonated $Glu^{131}$ serves as a general acid for proton transfer to the hydroxyl leaving group upon glycosidic cleavage. The optimal pH of the enzyme of ≈4.0 is close to the $pK_a$ for the γ-carboxylate of free glutamic acid, which supports its ability to serve subsequently as a general base to deprotonate and activate incoming water for hydrolysis. Glutamine lacks dissociable protons and is therefore incapable of substituting as a general acid/base. During catalysis, the substrate acetamido group becomes polarized for nucleophilic attack at the anomeric carbon, developing a positive charge on the amide nitrogen while forming the oxyanion nucleophile. $Asp^{129}$ must preserve its negative charge to facilitate polarization by neutralizing the positive charge on the nitrogen.

$Tyr^{247}$ was also an essential residue in our analysis. Placement of $Tyr^{247}$ in the structural model suggests its role is to coordinate and stabilize the oxyanion during transition state formation: the hydroxyl of $Tyr^{247}$ is optimally located for hydrogen bond donation to the carbonyl oxygen. An inert role in binding is less likely, because the Y247F mutation preserves the hydrophobic character of the residue that is thought to be important for association with sugar rings in the substrate. Structural inspection predicts $Ser^{245}$ does not contact the substrate directly but that the side chain hydroxyl would be an essential linchpin between $Tyr^{202}$ and $Tyr^{247}$, forming a hydrogen bond with the hydroxyl of $Tyr^{202}$ and the *pi* cloud of $Tyr^{247}$ and thereby positioning them both. This is consistent with the comparable $V_{max}$ but reduced apparent substrate binding of both the Y202F and S245A mutants.

The $Arg^{265}$ guanidino forms a salt bridge with the side chain carboxylate of $Asp^{206}$ in the crystal structure of human Hyal1. Interestingly, this interaction bridges two strands of "unstructured" coil that shape the active site of the enzyme. One of these strands, containing $Asp^{206}$, positions $Tyr^{202}$ optimally for binding to the substrate during catalysis. The other strand orients $Ser^{245}$ and the essential $Tyr^{247}$, exact placement of which is critical for transition state formation. Thus, instead of implicating the arginine directly in substrate binding via salt bridging with the carboxylate moieties, as was previously postulated for an analogous mutation in PH-20, the R265L mutation in Hyal1 shows its importance for structural integrity. The magnitude of its effect on catalysis also suggests the shape and rigidity of the active site cavity is critical to its function, regardless of the presence of specific catalytic residues.

Despite the essential interaction of $Asp^{206}$ with $Arg^{265}$ in active site architecture, a disulfide between $Cys^{207}$ and $Cys^{221}$, which holds the coil strand containing $Asp^{206}$ and $Tyr^{202}$ in contact with the next adjacent coiled strand to form a loop with $Asn^{216}$ at the apex, is apparently not required for Hyal1 activity. This loop may be stabilized by other interactions and/or not directly involved in substrate binding or catalysis. Furthermore, because this loop is the most remote of the contiguous secondary backbone elements that form the active site crevice, it may have the most structural and conformational fluidity. This would be consistent with the relatively high mobility in the structure of this region. It is interesting to find that disulfides in general are only essential for hyaluronidase activity in substrate gel assays. One major difference between this assay format and the microplate or Morgan-Elson color reaction formats is that the proteins are first denatured by SDS and immobilized in an acrylamide matrix for the substrate gel, presumably limiting their conformational mobility, whereas native, soluble protein is analyzed in the quantitative assays. This result suggests that disulfides assist the adoption of native folded structure and are essential to the partial refolding that allows hyaluronidase to function upon renaturation by removal of SDS from the substrate gel. Because the native structure is not disrupted in microplates, disulfides are not required for short term folded structures and therefore appear irrelevant to protein activity.

Prior studies of Hyal1 and PH-20 revealed reduced activity in solution and substrate gel assays, respectively, upon partial enzymatic removal of *N*-glycosides (24, 38). However, complete digestion was not achieved. The results reported here provide the first direct temporal link between the kinetics of deglycosylation and the loss of hyaluronidase activity. In addition, this analysis has shown definitively that Hyal1 lacks activity in the absence of glycosylation, whether resulting from glycoside removal post-purification or from expression as a point mutant incapable of being glycosylated at a specific residue. We were able to follow glycoside removal by changes in the molecular mass of Hyal1 by Western blot, in which an apparent 52-kDa band in untreated samples was presumed to be fully glycosylated, whereas a shift to two bands of ≈42 and 45 kDa was consistently the end product of PNGase treatment and likely is fully deglycosylated. Two bands may indicate that one species retains the 22-amino acid signal peptide and the other has had it cleaved. The fourth band seen in significant quantity is an intermediate species that appears in the N216A lysate and is the identical size of the N350A mutant, thus this is probably deglycosylated only at position 350. Because the N350A mutant completely lacked activity, deglycosylation at $Asn^{350}$ is probably the most detrimental to activity.

Lysosomal enzymes are commonly glycosylated (39), presumably to protect the protein in the acidic environment of this compartment, conditions under which Hyal1 is optimally active. The region of Hyal1 that contains $Asn^{350}$ is relatively mobile as indicated by the crystallographic data, but extensive contact between the sugar modifications and the secondary structural elements may be important for maintaining stability of the overall folded structure of the protein indirectly. The possibility exists that glycosyl adducts could facilitate catalysis directly by promoting association with the polymeric HA substrate and increasing affinity. However, the kinetic analysis showed that activity of deglycosylated Hyal1 at all time points was still saturable with increasing substrate concentration, but that $V_{max}$ was reduced. If glycosylation state only affected affinity, maximal rate of catalysis would not be expected to change.

$Asn^{350}$ was modeled in the structure with a hexasaccharide adduct that was fitted to visible electron density, which further supports its primary role in structural integrity relative to the other glycosylation sites. No electron density was present for $Asn^{216}$ modification so either this residue is not modified or high mobility in this region obscures additional atoms from view. Support for $Asn^{216}$ modification derives from the observation that the N216A mutant is partly secreted and active, but intracellularly about 50% of the protein is a species that lacks the ≈4-kDa adduct, such that it is the same size as N350A on a Western blot. Thus, glycosylation at position $Asn^{216}$ may not be extensive but may facilitate folding and maturation. The side chain of $Asn^{216}$ is modeled as oriented to the solvent accessible surface of the enzyme, with no obvious requisite interactions, but it may nonetheless interact with HA itself, which would explain the difference in $K_m$ between wild-type and N216A Hyal1. $Asn^{99}$ is modeled with two sugar adducts. This highly mobile region is directed outward and remote from the active site and may be less structurally critical, perhaps lacking extensive contact within the main domain.

It has been proposed that the C-terminal EGF-like domain, found in several reported splice variants of Hyal1, may be the site of as yet undefined protein-protein interactions (27). The results presented here suggest that such interactions would have to occur specifically with the solvent-exposed surface of the domain, because the inactivity of the truncated mutants and their inability to be secreted imply that this region does not function as an independently folded domain. Its homology to EGF may be a coincidental folding motif. However, numerous extracellular matrix proteins, such as laminin, that bear similar domains have been shown to activate EGF-type signaling although they do not compete directly with EGF for cell surface binding (35).

The analysis of Hyal1 point mutants highlights the importance of specific conserved residues in catalytic function, but also identifies active site conformation as a critical factor. Disrupted activity resulted from the R265L mutation but not from N216A or global disulfide reduction. Because each of these perturbations has the potential to impact structural integrity of the enzyme and each is located in positions of potential direct contact with bound substrates, the differences suggest areas of lesser or greater mobility within the protein may be important for the accommodation of diverse HA substrate sizes. Inspection of the Hyal1 solvent-accessible surface according to its crystal mobility reveals an N-terminal domain encompassing residues from $Pro^{62}$ to $Pro^{205}$ that displays higher collective structural mobility. This suggests that the N-terminal portion may move as an entity relative to the remainder of the protein, like a closing finger and thumb. The thumb appears to be the similarly mobile loop containing $Asn^{216}$. Together the closing appendages may regulate clasping of polymeric HA substrates and release of cleaved products. In contrast, residues in the active site groove, and the hydrophobic folded core of the protein, exhibit the least mobility. At least two residues partially obscure the substrate solvent accessibility and are among the residues with the least motion. One of these is a tryptophan (residue 321) that makes van der Waals contact with the bound carbon rings and the other is $Tyr^{247}$, which interacts with the acetamide of the newly cleaved substrate. This is consistent with a well defined active site conformation that constrains the bound ligand for catalysis, whereas the mobile regions allow promiscuity in polymeric length of the substrate.

## REFERENCES


1. Jedrzejas, M. J., and Stern, R. (2005) *Proteins* **61,** 227–238
2. Stern, R., and Jedrzejas, M. J. (2006) *Chem. Rev.* **106,** 818–839
3. Csoka, A. B., Frost, G. I., and Stern, R. (2001) *Matrix Biol.* **20,** 499–508
4. Markovic-Housley, Z., Miglierini, G., Soldatova, L., Rizkallah, P. J., Muller, U., and Schirmer, T. (2000) *Structure* **8,** 1025–1035
5. Triggs-Raine, B., Salo, T. J., Zhang, H., Wicklow, B. A., and Natowicz, M. R. (1999) *Proc. Natl. Acad. Sci. U. S. A.* **96,** 6296–6300
6. Kovar, J. L., Johnson, M. A., Volcheck, W. M., Chen, J., and Simpson, M. A. (2006) *Am. J. Pathol.* **169,** 1415–1426
7. Liu, D., Pearlman, E., Diaconu, E., Guo, K., Mori, H., Haqqi, T., Markowitz, S., Willson, J., and Sy, M. S. (1996) *Proc. Natl. Acad. Sci. U. S. A.* **93,** 7832–7837
8. Shiftan, L., Israely, T., Cohen, M., Frydman, V., Dafni, H., Stern, R., and Neeman, M. (2005) *Cancer Res.* **65,** 10316–10323
9. Shiftan, L., and Neeman, M. (2006) *Contrast Media Mol. Imaging* **1,** 106–112

10. West, D. C., Hampson, I. N., Arnold, F., and Kumar, S. (1985) *Science* **228,** 1324–1326
11. West, D. C., and Kumar, S. (1989) *Exp. Cell Res.* **183,** 179–196
12. West, D. C., and Kumar, S. (1989) *Ciba Found. Symp.* **143,** 187–201; Discussion, 201-187, 281-185
13. Simpson, M. A. (2006) *Am. J. Pathol.* **169,** 247–257
14. Lokeshwar, V. B., Cerwinka, W. H., Isoyama, T., and Lokeshwar, B. L. (2005) *Cancer Res.* **65,** 7782–7789
15. Coutinho, P. M., and Henrissat, B. (1999) in *Recent Advances in Carbohydrate Bioengineering* (Gilbert, H. J., Davies, G., Henrissat, B., and Svensson, B., eds) pp. 3–12, The Royal Society of Chemistry, Cambridge
16. Davies, G. J., Gloster, T. M., and Henrissat, B. (2005) *Curr. Opin. Struct. Biol.* **15,** 637–645
17. Rye, C. S., and Withers, S. G. (2000) *Curr. Opin. Chem. Biol.* **4,** 573–580
18. Drouillard, S., Armand, S., Davies, G. J., Vorgias, C. E., and Henrissat, B. (1997) *Biochem. J.* **328,** 945–949
19. Piszkiewicz, D., and Bruice, T. C. (1968) *J. Am. Chem. Soc.* **90,** 2156–2163
20. Rao, V., Cui, T., Guan, C., and Van Roey, P. (1999) *Protein Sci.* **8,** 2338–2346
21. Terwisscha van Scheltinga, A. C., Armand, S., Kalk, K. H., Isogai, A., Henrissat, B., and Dijkstra, B. W. (1995) *Biochemistry* **34,** 15619–15623
22. Hofinger, E. S., Bernhardt, G., and Buschauer, A. (2007) *Glycobiology* **17,** 963–971
23. Hofinger, E. S., Hoechstetter, J., Oettl, M., Bernhardt, G., and Buschauer, A. (2008) *Glycoconj. J.* **25,** 101–109
24. Hofinger, E. S., Spickenreither, M., Oschmann, J., Bernhardt, G., Rudolph, R., and Buschauer, A. (2007) *Glycobiology* **17,** 444–453
25. Arming, S., Strobl, B., Wechselberger, C., and Kreil, G. (1997) *Eur. J. Biochem.* **247,** 810–814
26. Botzki, A., Rigden, D. J., Braun, S., Nukui, M., Salmen, S., Hoechstetter, J., Bernhardt, G., Dove, S., Jedrzejas, M. J., and Buschauer, A. (2004) *J. Biol. Chem.* **279,** 45990–45997
27. Chao, K. L., Muthukumar, L., and Herzberg, O. (2007) *Biochemistry* **46,** 6911–6920
28. Sramkoski, R. M., Pretlow, T. G., 2nd, Giaconia, J. M., Pretlow, T. P., Schwartz, S., Sy, M. S., Marengo, S. R., Rhim, J. S., Zhang, D., and Jacobberger, J. W. (1999) *In Vitro Cell Dev. Biol. Anim.* **35,** 403–409
29. Huang, C. C., Couch, G. S., Pettersen, E. F., and Ferrin, T. E. (1996) *Pacific Symp. Biocomput.* **1,** 724
30. Blom, N., Sicheritz-Ponten, T., Gupta, R., Gammeltoft, S., and Brunak, S. (2004) *Proteomics* **4,** 1633–1649
31. Prasad, A. R., Nishimura, J. S., and Horowitz, P. M. (1983) *Biochemistry* **22,** 4272–4275
32. Lokeshwar, V. B., Lokeshwar, B. L., Pham, H. T., and Block, N. L. (1996) *Cancer Res.* **56,** 651–657
33. Bharadwaj, A. G., Rector, K., and Simpson, M. A. (2007) *J. Biol. Chem.* **282,** 20561–20572
34. Frost, G. I., and Stern, R. (1997) *Anal. Biochem.* **251,** 263–269
35. Engel, J. (1989) *FEBS Lett.* **251,** 1–7
36. Reissig, J. L., Storminger, J. L., and Leloir, L. F. (1955) *J. Biol. Chem.* **217,** 959–966
37. Bharadwaj, A. G., Kovar, J. L., Loughman, E., Elowsky, C., Oakley, G. G., and Simpson, M. A. (2009) *Am. J. Pathol.* **174,** 1027–1036
38. Li, M. W., Yudin, A. I., Robertson, K. R., Cherr, G. N., and Overstreet, J. W. (2002) *J. Androl.* **23,** 211–219
39. Ohtsubo, K., and Marth, J. D. (2006) *Cell* **126,** 855–867

Supplementary figure 1. Intrinsic tryptophan fluorescence of native and denatured Hyal1. Purified Hyal1 wild-type (WT) and each of the inactive point mutants was evaluated for structural integrity by fluorescence scanning following tryptophan excitation at 295 nm. Spectra were collected on 50 nM protein in a buffer of 50 mM tris-HCl, pH 7.0, and 150 mM NaCl in the absence (native) or presence (denatured) of 3M guanidine-HCl as indicated. All spectra were recorded following a 3 min incubation at room temperature.

Supplemental Table 1. Primer sequences for Hyal1 site-directed mutagenesis

| Primer Label | Primer Sequence |
|---|---|
| Hy1wt Forward | TGACAAGCTTTTTAGGGGCCCCTTGC |
| Hy1wt Reverse | CTGAGAATTCTCACCACATGCTCTTC |
| D129N Forward | GGGCTGGCAGTCATCAACTGGGAGGCATGGC |
| D129N Reverse | GCCATGCCTCCCAGTTGATGACTGCCAGCCC |
| E131Q Forward | GCAGTCATCGACTGGCAGGCATGGCGCCCAC |
| E131Q Reverse | GTGGGCGCCATGCCTGCCAGTCGATGACTGC |
| Y202F Forward | GGCCTCTGGGGCTTCTTTGGCTTCCCTGACT |
| Y202F Reverse | AGTCAGGGAAGCCAAAGAAGCCCCAGAGGCC |
| S245A Forward | CGTGCCCTCTATCCCGCCATCTACATGCCCG |
| S245A Reverse | CGGGCATGTAGATGGCGGGATAGAGGGCACG |
| Y247F Forward | CTCTATCCCAGCATCTTCATGCCCGCAGTGC |
| Y247F Reverse | GCACTGCGGGCATGAAGATGCTGGGATAGAG |
| R265L Forward | ATGTATGTGCAACACCTTGTGGCCGAGGCAT |
| R265L Reverse | ATGCCTCGGCCACAAGGTGTTGCACATACAT |
| N216A Forward | CTATGACTTTCTAGGCCCCGCCTACACCGGCCAGTGC |
| N216A Reverse | GCACTGGCCGGTGTAGGCGGGGCCTAGAAAGTCATAG |
| N350A Forward | TACACTGGGGCCCTTCATCCTGGCCGTGACCAGTGGGGC |
| N350A Reverse | GCCCCACTGGTCACGGCCAGGATGAAGGGCCCCAGTGTA |
| N350tr Forward | GGGCCCTTCATCCTGTAGGTGACCAGTGGGGCC |
| N350tr Reverse | GGCCCCACTGGTCACCTACAGGATGAAGGGCCC |
| L356tr Forward | GTGACCAGTGGGGCCTGACTCTGCAGTCAAGCC |
| L356tr Reverse | GGCTTGACTGCAGAGTCAGGCCCCACTGGTCAC |

Zhang, et al, Supplemental Figure 1